

SURFACE-BASED IN SITU AND VERTICALLY-POINTING MEASUREMENTS
OF PRECIPITATION CHARACTERISTICS NEAR AND WITHIN THE MELTING LAYER
OBTAINED AT MCKENZIE BRIDGE, OREGON DURING IMPROVE II

Sandra E. Yuter*
University of Washington, Seattle, WA

Louisa B. Nance
CIRES/NOAA/ETL, Boulder, CO

Martin Löffler-Mang
University of Applied Sciences, Saarbrücken, Germany

1. INTRODUCTION

Within cold precipitating clouds, a melting layer containing a combination of rain, ice, and partially melted particles exists between layers of ice particles above and rain below. The vertical extent of the melting layer is a function of the dynamical and microphysical environments. Small ice particles and weak vertical air velocities (< fall speed of ice) are associated with thinner layers, whereas large rimed ice particles and strong vertical air velocities (> fall speed of ice) are associated with thicker layers. The melting of aggregates in an environment of weak vertical air velocities is observed by radar as a “bright band” in reflectivity and as a sharp discontinuity in vertically-pointing Doppler velocity. In such conditions, the melting layer often contains a 0°C isothermal layer 10’s of meters thick. Turbulence has been observed within the melting layer itself and wind shear may be evident at its upper boundary (Steiner et al. 2003). The goal of this study is to quantify the particle size distributions of ice and rain particles within and just below a well-defined melting layer. Better physical understanding of the details of the melting layer will aid in the refinement of microphysical parameterizations for numerical models and in physical interpretation of remote sensing measurements at microwave and radar frequencies.

2. DATA

As part of IMPROVE II (Stoelinga et al. 2003), a suite of instrumentation was deployed at McKenzie Bridge, Oregon in the foothills of the Oregon Cascades including NOAA ETL’s vertically-pointing S-band Doppler radar (White et al. 2000), a 915 MHz wind profiler (Weber et al. 1993), and a suite of surface meteorology instrumentation. Among the surface instruments was a PMTech Inc. PARSIVEL M300 disdrometer which simultaneously measures particle

size and fall velocity (Löffler-Mang and Joss 2000). The PARSIVEL can measure particles with diameters from about 0.3 to 24 mm and fall velocities from 0.25 to 21 m/s. The PARSIVEL data were quality-controlled following a procedure defined by U. Blahak (personal communication). Particles larger than ~2.5 mm are difficult to observe with aircraft probes because of sample volume and turbulence constraints. Hence, PARSIVEL surface-based in situ data provide a means of quantifying the number of large aggregates within the melting layer. By comparing the joint probability distribution of size and fall velocity for the observed particles to empirical size-fall speed relations for rain and different types of ice particles, a classification of the particles into rain and not-rain categories can be made.

3. 18-19 DECEMBER 2001 STORM

The McKenzie Bridge site experienced several periods when the melting layer between ice and rain intersected the surface. We examine such a period during the 18-19 December 2001 storm. Figure 1 shows the time series of temperature and estimated rain rate during the storm. Several pulses of rainfall occurred during this period corresponding to pre- and post-frontal rainbands. From 2030 UTC to 2345 UTC the temperature dropped from 1.5°C to 0.5°C (segment A in Fig. 1) and from 2346 UTC – 0049 UTC it decreased from 0.5°C to 0°C (segment B in Fig. 1). The temperature then remained steady at 0 °C for ~10 hours during which precipitation associated with the interior of the melting layer fell for nearly 7 hours (segment C in Fig. 1). The vertically-pointing reflectivity data in Figure 2 shows the decreasing altitude and then disappearance of the bright band as it drops below the lowest range gate of the radar and then intersects the surface. The hourly averaged profiles of horizontal wind velocity shown in Figure 3 indicate a near surface wind shift from southerly to westerly as the front passed at about 18 UTC but little wind shear within the vertical columns containing the melting layer.

* *Corresponding author address:* Sandra E. Yuter, Univ. of Washington, Dept. of Atmospheric Sciences, Seattle, WA 98195; e-mail: yuter@atmos.washington.edu.

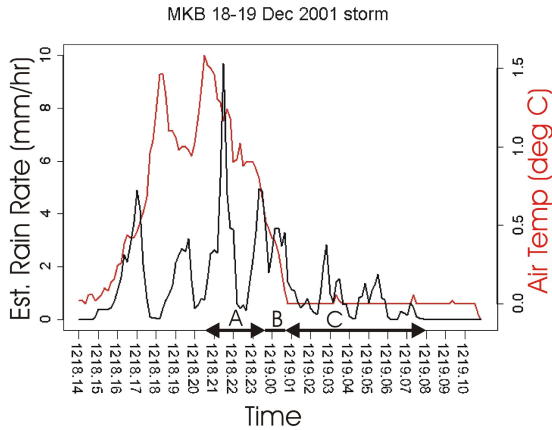


Figure 1. Time series of 10-min averaged surface air temperature (red) and PARSIVEL estimated rain rate (black) assuming the detected particles are all rain for 14 UTC 18 December to 10 UTC 19 December 2001. Line segments A, B, and C indicate the time periods of the temperature regimes defined in the text.

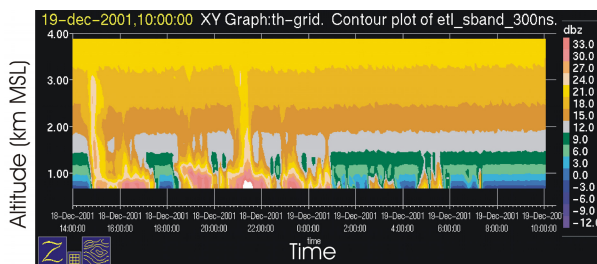


Figure 2. Time-height plot of reflectivity obtained by NOAA/ETL vertically-pointing S-band radar using its 300 ns coupled operating mode for time period in Figure 1.

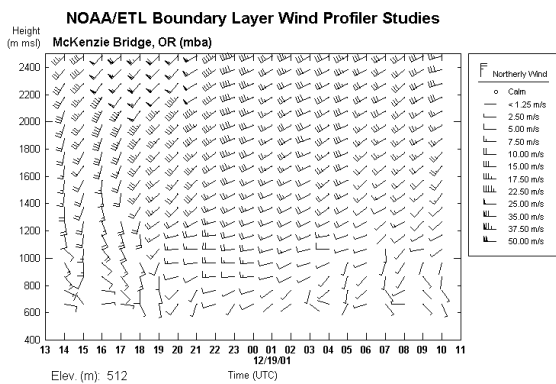


Figure 3. Time height section of hourly averaged horizontal wind profiles from the NOAA/ETL 915-MHz wind profiler for time period in Figure 1.

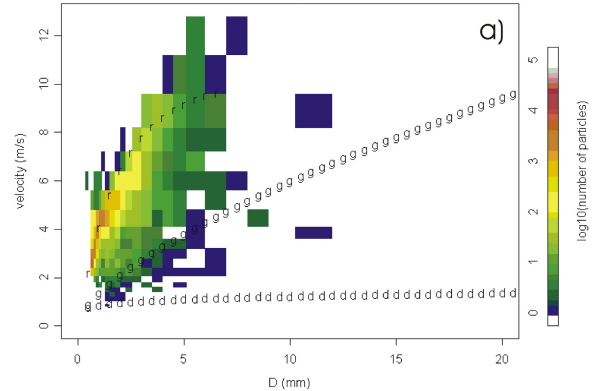
4. ANALYSIS

4.1 Particle Size and Fall Speed

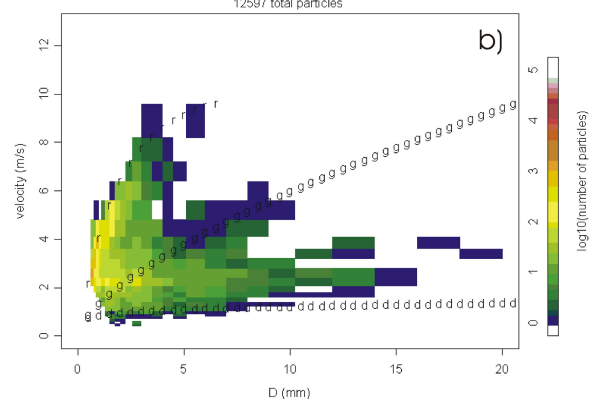
Figure 4 presents the PARSIVEL data for time segments A, B, and C from Figure 1 as matrixes with particle diameter on the x-axis and fall speed on the y-

axis. Overlaid on each of the plots are the curves for the empirical fall speed relation for rain (r) obtained by Gunn and Kinzer (1949) and the relations for lump graupel (g) and unrimed dendrites (d) obtained by Locatelli and Hobbs (1974).

PARSIVEL matrix 20011218 2030 - 2345 falling temp 1.5 - 0.5 deg C
33679 total particles



PARSIVEL matrix 20011218 2346 - 0049 falling temp 0.5 - 0 deg C
12597 total particles



PARSIVEL matrix 20011219 0050-0800 steady temp 0 deg C
27356 total particles

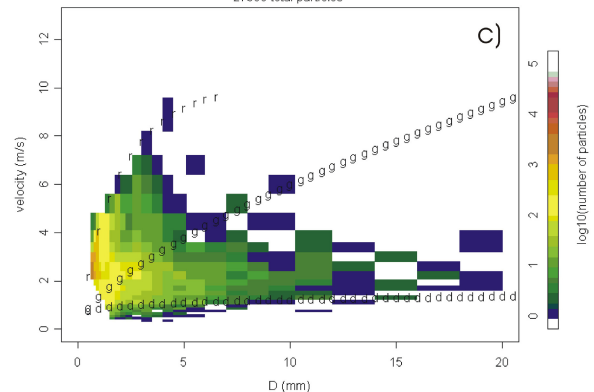


Figure 4. Matrix of PARSIVEL particle diameter and fall speed for a) Segment A: 2030-2345 UTC, 33679 particles, b) Segment B: 2346-0049 UTC, 12597 particles, and c) Segment C: 0050-0800 UTC, 27356 particles. The number of particles in each individual size-fall speed bin is color-coded according to the \log_{10} of the number of particles in the bin.

During segment A (Fig. 4a), when the temperature dropped from 1.5°C to 0.5°C, most of the particles occur near the rain curve and are likely rain. The subset of the particles that lie between the rain and graupel curves have slower velocities for a given size compared to rain but are falling faster than graupel. This subset is likely partially melted particles. In segment B (Fig. 4b), the temperature drops from 0.5°C to 0°C and a bimodal distribution is evident with a larger subset of the particles centered near the rain curve and a smaller subset near but falling slightly faster than the dendrite curve. Both rain and snow coexist. During segment C (Fig. 4c), rain is still evident but relatively more snow particles occur including individual snow particles up to 20 mm diameter.

4.2 Particle Size Distributions for Rain and Not-Rain

A partition of the particles into rain and not-rain subsets is made by categorizing the particles near the rain curve as “rain” (Figure 5a) and all other particles as “not rain” (Figure 5b). These subsets are then summed for each size bin to obtain traditional plots of particle size distribution shown in Figure 6.

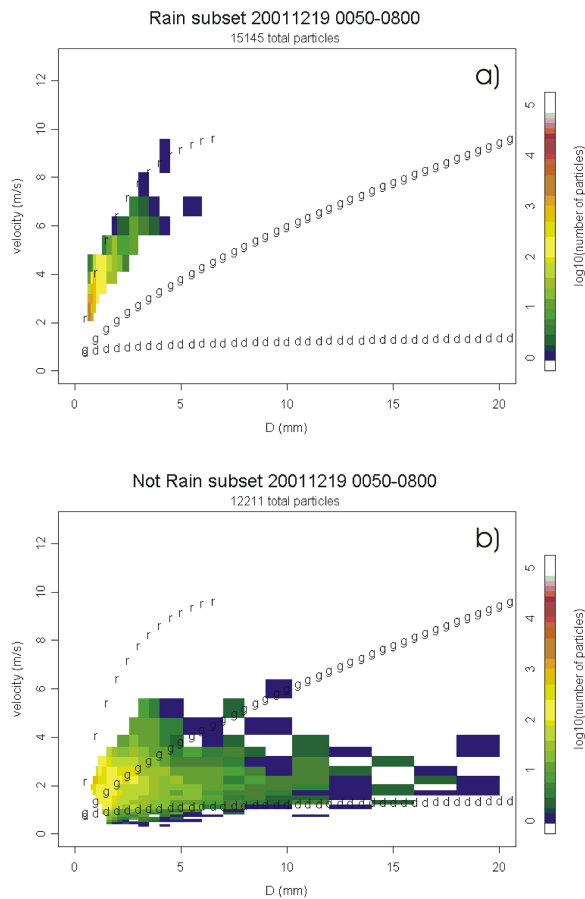


Figure 5. Classified rain and not rain subsets of particles for segment C, corresponding to Figure 4c.

Data obtained while temperatures were steady at 0°C correspond to particles within the interior of the melting layer while data obtained between 0.5°C to 0°C correspond to the region just below the altitude of the melting layer. The distributions are roughly exponential (i.e. linear in D-log₁₀(N) space) for the rain and not-rain particles below the melting layer (Figs. 6c and d). Within the melting layer, there is a tendency for larger not-rain particles to occur in quantities more numerous than an exponential distribution would predict (Fig. 6b). The ratio of rain to not-rain particles doubles from 1.2 within the melting layer to 2.4 below the melting layer. At temperatures > 0.5°C (not shown), few large aggregates (> 5 mm) persist. They have likely completely or partially melted and collapsed to a smaller size before reaching 0.5°C.

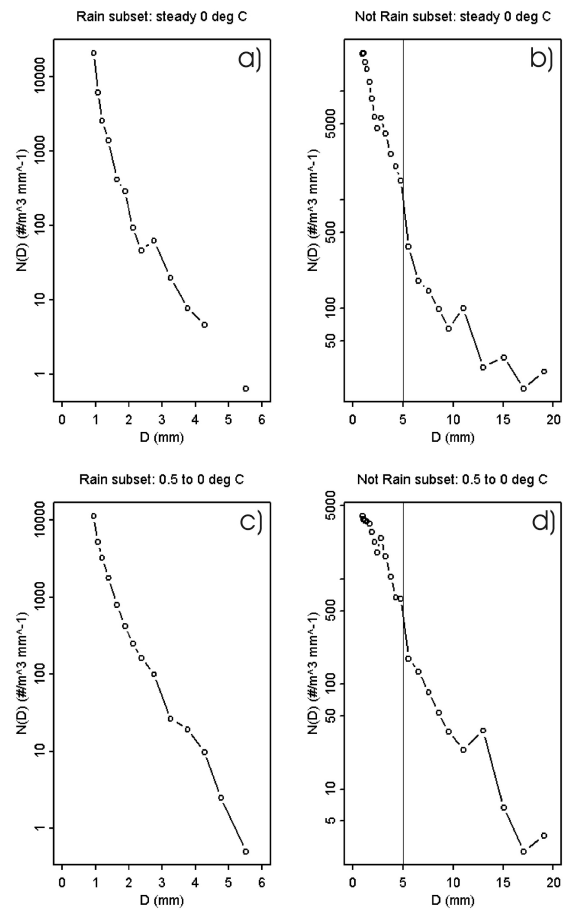


Figure 6. Particle size distributions for rain and not-rain subsets of particles. For segment C, within melting layer a) rain and b) not-rain. For segment B, just below melting layer, c) rain and d) not-rain. Vertical line in b) and c) corresponds to 5 mm diameter. Scale of y-axis varies between subplots. X-axis maximum varies from 6 mm to 20 mm between rain and not-rain plots.

5. CONCLUSIONS

Previous studies of the melting layer have utilized vertically-pointing radar and modeling to characterize its microphysics. Remote sensing methods have ambiguities in interpretation of data from resolution volumes containing mixed precipitation when the size distributions of the ice and rain components are unknown. Data from in situ aircraft measurements is primarily limited to particles < 2.5 mm diameter and cannot completely resolve this ambiguity. In their study, Fabry and Zawadzki (1995) found that the change in dielectric factor followed by a change in fall speed accounted for only about half of the observed reflectivity enhancement in the melting layer. Our data suggest that aggregation within the isothermal layer, particularly of large particles > 5 mm diameter, may be enhanced. Since reflectivity is the 6th moment of diameter (D^6), the contribution by individual particles of 5 mm and 20 mm diameter differs by a factor of 4096. We speculate that a small number of very large wet aggregates (> 10 mm) may account for most of the missing portion of the reflectivity within the melting band. Additional surface-based data sets which include precipitation from below, within, and above the melting layer (the latter is not available in our dataset) need to be collected and analyzed to resolve this issue.

Acknowledgements:

Gratefully appreciated are the help and advice of Ulrich Blahak, David Kingsmill, Daniel Gottas and Allen White. Special thanks to University of Karlsruhe and PMTech Inc. for the loan of the PARSIVEL disdrometer. The work of the first author was supported by NSF grant ATM-0121963 and NASA TRMM grant NAG5-9750.

References

- Fabry, F., and I. Zawadzki, 1995: Long-term radar observations of the melting layer of precipitation and their interpretation. *J. Atmos. Sci.*, **52**, 838-851.
- Gunn, R., and G. D. Kinzer, 1949: The terminal velocity of fall for water droplets in stagnant air. *J. Meteor.*, **6**, 243-248.
- Locatelli, J. D., and P. V. Hobbs, 1974: Fall speeds and masses of solid precipitation particles. *J. Geophys. Res.*, **79**, 2185-2197.
- Löffler-Mang, M., and J. Joss, 2000: An optical disdrometer for measuring size and velocity of hydrometeors. *J. Atmos. Ocean. Tech.*, **17**, 130-139.
- Steiner, M., O. Bousquet, R. A. Houze, Jr., B. F. Smull, and M. Mancini, 2003: Airflow within major alpine river valleys under heavy rainfall. *Quart. J. Roy. Meteor. Soc.*, **129**, 411-431.
- Stoelinga, M., P. V. Hobbs, C. F. Mass, J. D. Locatelli, B. A. Colle, R. A. Houze, Jr., A. L. Rangno, N. A. Bond, B. F. Smull, R. M. Rasmussen, G. Thompson, and B. Colman, 2003: Overview of IMPROVE: Verification and improvement of bulk microphysical parameterizations in mesoscale models., Preprints, AMS Mesoscale Conference, Portland, OR.
- Weber, B. L., D. B. Wuertz, D.C. Welsh, R. McPeck, 1993: Quality controls for profiler measurements of winds and RASS temperatures. *J. Atmos. Ocean. Tech.*, **10**, 452-464.
- White, A. B., J. R. Jordan, B. E. Martner, F. M. Ralph, and B. W. Bartram, 2000: Extending the dynamic range of an S-band radar for cloud and precipitation studies. *J. Atmos. Ocean. Tech.*, **17**, 1226-1234.